Phase-Locking of Second-Harmonic Gyrotrons for Providing MW-Level Output Power

G. G. Denisov, I. V. Zotova, I. V. Zheleznov, A. M. Malkin, N. S. Ginzburg, A. S. Sergeev, E. S. Semenov, and M. Yu. Glyavin

***Abstract*— We propose the method of providing megawatt (MW)-level output power in continuous wave (CW) or long-pulse second-harmonic (SH) gyrotrons using phase-locking by a weak external monochromatic signal. Typically, the power of harmonic gyrotrons is hindered due to excitation of spurious fundamental-harmonic modes at the front of the accelerating voltage and the beam current. Injection of a seeding signal at the operating SH mode (priming) can suppress the spurious generation during the startup process. Within the frame of a self-consistent multimode model, we demonstrate the applicability of this approach to provide ~1-MW radiation in a 230-GHz SH gyrotron with the high-order $TE_{34,14}$ operating mode which is standardly unattainable for harmonic operation.**

***Index Terms*— High-power subterahertz (THz) gyrotrons, phase and frequency locking, second-harmonic (SH) generation.**

I. Introduction

AT PRESENT, the gyrotrons are the most powerful sources of coherent millimeter and submillimeter waves capable of operating in long-pulse and continuous wave (CW) regimes with megawatt (MW) power levels [1], [2]. The important application of high-power gyrotrons is plasma heating and current drive in controlled thermonuclear fusion installations [3], [4]. Such systems typically use gyrotrons of the short-wavelength part of the millimeter range (the generation frequency of 110–170 GHz) operating at the first (fundamental) cyclotron harmonic. The modern challenge in the development of high-power gyrotrons is associated with a significant increase in their operating frequency, which is in demand, for example, in next generation of tokamaks with a strong magnetic field planned for construction [5], [6]. Some progress in these studies was achieved recently in fundamental-harmonic (FH) gyrotrons [7], [8]. However, presently, this progress is restrained by the problem of creating strong magnetic fields in volumes, sufficient for installing high-power gyrotrons equipped with a large-diameter cathode.

Undoubtedly, it is attractive to use generation at the second cyclotron harmonic for increasing the frequency, which provides proportional reduction of the guiding magnetic field. According to the theoretical considerations [9], the maximum electron efficiency of second-harmonic (SH) gyrotrons in the single-mode approximation is close to that of gyrotrons based on the fundamental cyclotron resonance. However, the output power of experimentally implemented high-frequency SH gyrotrons does not exceed several tens of kilowatts with efficiency restricted by 20% [10]. The main problem that hinders obtaining a high power of SH radiation is competition with modes excited by the beam at the fundamental resonance. Moreover, spurious FH modes can be excited at the smooth front of the accelerating voltage and the beam current and, then, continue to exist in the steady-state regime suppressing the operating SH mode.

It should be noted that there are some approaches to solve the described problem [11]–[15] aimed at increasing the starting currents of parasitic FH modes, as well as selecting the gyrotron startup scenario for earlier excitation of the operating SH mode. However, these methods were mainly considered for sufficiently low transverse modes. At the same time, for high-power high-frequency generation, operation at high-order transverse modes is needed for reducing the Ohmic load. Note that the requirement for high power in CW or long pulse regimes makes it highly undesirable electrodynamics selection methods using irregularities in the gyrotron cavity [13], [14]. Simultaneously, electronic selection methods based on axial-encircling [15] or additional absorbing [12] electron beams contradict the requirement for high efficiency.

At the same time, the well-known and currently actively investigated method of spurious modes suppression for FH gyrotrons is associated with locking by an external weak monochromatic signal with the frequency and structure of the operating mode [16]–[20]. In the startup process, such a signal can provide priming the desired mode and helps this mode to suppress the competitors [18]. Moreover, according to recent studies [20], frequency-locking also provides a noticeable increase in efficiency, radiation power, and improvement

Manuscript received September 9, 2021; revised October 25, 2021 and December 2, 2021; accepted December 7, 2021. Date of publication December 20, 2021; date of current version January 24, 2022. This work was supported by the Russian Science Foundation (RSF) under Project 19-79-30071. The review of this article was arranged by Editor L. Kumar. *(Corresponding author: M. Yu. Glyavin.)*

G. G. Denisov, I. V. Zotova, I. V. Zheleznov, N. S. Ginzburg, A. S. Sergeev, E. S. Semenov, and M. Yu. Glyavin are with the FSBSI Federal Research Center, Institute of Applied Physics, Russian Academy of Sciences, 603950 Nizhny Novgorod, Russia (e-mail: glyavin@appl.sci-nnov.ru).

A. M. Malkin is with the FSBSI Federal Research Center, Institute of Applied Physics, Russian Academy of Sciences, 603950 Nizhny Novgorod, Russia, and also with the Radiophysics Department, Nizhny Novgorod State University, 603950 Nizhny Novgorod, Russia.

Color versions of one or more figures in this article are available at https://doi.org/10.1109/TED.2021.3134187.

Digital Object Identifier 10.1109/TED.2021.3134187

of generation stability of FH gyrotrons. This article applies this method to SH subterahertz (THz) gyrotrons to provide single-mode single-frequency generation with MW-level output power. This way does not require any essential modification of the device or a complicated startup scenario. Note, however, that the situation with the SH priming is complicated by the inherent for such gyrotrons nonlinear effect, when the excited harmonic facilitates the excitation of parasitic modes at the fundamental frequency [21]–[23]. Nevertheless, for considered area of parameters, this effect was not observed; thus, as will be shown below, weak external signal may provide priming of the desired mode, and its oscillations will remain stable with respect to all possible competitors.

This article is organized as follows. In Section II, we describe the basic multimode model of electron–wave interaction, taking into account the startup process and priming by an external signal. Since the quality factors of high-power gyrotrons' cavities are fairly low, the model with the self-consistent axial profile of the RF field is used in contrast with previous considerations [19]. In Section III, as an example of applicability of the proposed approach, we consider a possibility of MW-level SH generation in a 230-GHz gyrotron with the $TE_{34,14}$ operating mode.

II. Multimode Self-Consistent Model of a Gyrotron Operating in Frequency-Locking Regime

Theoretical analysis presented further is based on the model of low-Q cavity gyrotrons with nonfixed axial mode structures. Such gyrotron can be described by the following self-consistent system of partial differential equations, which describes competition of many transverse modes excited at different cyclotron harmonics (cf., [24])

$$\begin{aligned} &i\frac{\partial^2 a_n}{\partial Z^2}+s_n\frac{\partial a_n}{\partial \tau}+(i\varepsilon_n(Z)+i\Delta_n+\rho_n)a_n \\ &\quad=i\frac{\alpha_I\alpha_\perp^{s_n}}{\alpha_{||}}\frac{I_n}{4\pi^2}\int_0^{2\pi}\int_0^{2\pi}p^{s_n}e^{i(m_n-s_n)\varphi}d\theta_0 d\varphi \\ &\frac{\partial p}{\partial Z}+\frac{\bar g^2}{4\alpha_{||}}\frac{\partial p}{\partial \tau}+i\frac{\alpha_\perp^2}{\alpha_{||}}p\left(|p|^2-1\right) \\ &\quad=i\sum_n\frac{\alpha_\perp^{s_n-2}}{\alpha_\gamma\alpha_{||}}a_n\left(p^*\right)^{s_n-1}e^{-i(m_n-s_n)\varphi}. \end{aligned} \tag{1}$$

Here, p is the complex transverse momentum of electrons normalized to its absolute value at the entrance of interaction space, $Z=\bar\beta_\perp^2\bar\omega_g z/2c\bar\beta_{||}$ and $\tau=\bar\beta_\perp^4\bar\omega_g t/8\bar\beta_{||}^2$ are dimensionless axial coordinate and time, respectively,

$$a_n=\frac{eA_n}{m_e c\bar\omega_g}\frac{s_n^{s_n}}{2^{s_n-1}s_n!}\frac{\bar\beta_\perp^{s_n-4}}{\bar\gamma}J_{m_n-s_n}(\nu_n R_b)$$

is the normalized amplitude of the nth mode TE_{m_n,q_n} excited at the cyclotron harmonic with number s_n at the frequency $\bar\omega_n^c\approx s_n\bar\omega_g$ where $\bar\omega_g$ is the relativistic gyrofrequency in the operating point chosen as the reference frequency, $\bar\beta_\perp=\bar V_\perp/c$ and $\bar\beta_{||}=\bar V_{||}/c$ are normalized electrons velocities, $\bar g=\bar\beta_\perp/\bar\beta_{||}$ is the pitch-factor, $\bar\gamma\approx 1+e\bar U/m_e c^2$ is the relativistic factor, $\bar U$ is the accelerating voltage in the operating point (at the end of the startup process)

$$\bar I_n=64\frac{e\bar I_b}{m_e c^3}\frac{\bar\beta_{||}\bar\beta_\perp^{2(s_n-4)}}{\bar\gamma}s_n^3\left(\frac{s_n^{s_n}}{2^{s_n}s_n!}\right)^2\frac{J_{m_n-s_n}^2(\nu_n R_b)}{\left(\nu_n^2-m_n^2\right)J_{m_n}^2(\nu_n)}$$

is the normalized current parameter, $\bar I_b$ is the operating electron current, R_b is the injection radius, $J_{m_n}(x)$ is the Bessel function of the first order, m_n is the azimuthal index of the nth mode, ν_n is its eigenvalue, $\rho_n=s_n^2 4\beta_{||0}^2\beta_{\perp 0}^{-4}/Q_n^{\rm ohm}$ is the parameter of Ohmic losses, $Q_n^{\rm ohm}=Rd_n^{-1}(1-m_n^2\nu_n^{-2})$ is the Ohmic Q-factor, and d_n is the frequency-dependent skin depth. Function $\varepsilon_n(Z)=8\bar\beta_{||}^2 s_n^2(\bar\omega_n^c-\omega_n^c(Z))/\bar\omega_n^c\bar\beta_\perp^4$ describes the variation of the cutoff frequency $\omega_n^c(Z)=\nu_n c/R(Z)$ along z-axis, $R(Z)$ is the profile of the smoothly tapered gyrotron cavity, and $\bar\omega_n^c$ is the cutoff frequency in its regular part.

Unlike [24], the gyrotron startup is taken into account in (1) by slow variation of electron beam parameters (energy, current, axial, and transverse velocities) in the process of the accelerating voltage rising $U(\tau)$

$$\begin{aligned} \alpha_\gamma&=\frac{\gamma\left(U(\tau)\right)}{\bar\gamma},\quad \alpha_I(\tau)=\frac{I_b(U(\tau))}{\bar I_b} \\ \alpha_{||}(\tau)&=\frac{\beta_{||}(U(\tau))}{\bar\beta_{||}},\quad \alpha_\perp(\tau)=\frac{\beta_\perp(U(\tau))}{\bar\beta_\perp}. \end{aligned} \tag{2}$$

Function $\Delta_n(\tau)=8\bar\beta_{||}^2 s_n^2(s_n\bar\omega_g\alpha_\gamma^{-1}-\bar\omega_n^c)/\bar\omega_n^c\bar\beta_\perp^4$ describes startup variation of the cyclotron resonance detuning.

For diode-type magnetron-injection guns, temporal dependence of the pitch-factor and the current–voltage characteristic taking into account the Schottky effect are given by relations [25]

$$g(U(\tau))=\bar g\sqrt{\frac{U(\tau)}{\left(1+\bar g^2\right)\bar U-\bar g^2 U(\tau)}} \tag{3}$$

$$I_b(U(\tau))=\bar I_b e^{B\left(\sqrt{U}-\sqrt{\bar U}\right)}. \tag{4}$$

Equations (3) and (4) allow us to calculate the functions (2) introduced above. The coefficient B in (4) is found based on experimental current–voltage characteristics of modern high-power gyrotrons (see, for example, [26]).

Equation (1) has to be supplemented by proper boundary conditions. For motion equations, we apply standard conditions corresponding to electrons uniformly distributed over the cyclotron rotation phases at the entrance of the interaction space: $p(Z=0)=e^{i\theta_0}$, $\theta_0\in[0,2\pi)$. Note that we consider here interaction with a thin electron beam without velocity spread. For modes' amplitudes, boundary conditions are written in the form

$$\begin{aligned} &a_n(\tau,0)-\frac{1}{\sqrt{i\pi s_n}}\int_0^\tau\frac{e^{-i\Phi_n(\tau,\tau',0)}}{\sqrt{\tau-\tau'}}\frac{\partial a_n(\tau',0)}{\partial Z}d\tau' \\ &\quad=0 \end{aligned} \tag{5a}$$

$$\begin{aligned} &a_n(\tau,L)+\frac{1}{\sqrt{i\pi s_n}}\int_0^\tau\frac{e^{-i\Phi_n(\tau,\tau',L)}}{\sqrt{\tau-\tau'}}\frac{\partial a_n(\tau',L)}{\partial Z}d\tau' \\ &\quad=2\delta_{n,N}F_0 e^{i\Omega_n\tau+i\Phi_n(\tau,0,L)} \end{aligned} \tag{5b}$$

where $\delta_{n,N}$ is the Kronecker delta, $L=\bar\beta_{\perp 0}^2\bar\omega_H l_z/2\bar\beta_{||0}c$ is the normalized length of the

gyrotron cavity with the physical length l_z, and $\Phi_n(\tau, \tau', Z) = s_n^{-1} \int_{\tau'}^{\tau} (\Delta_n(\tau'') + \varepsilon_n(Z) - i\sigma_n) d\tau''$, F_0, and $\Omega_n = 8\bar{\beta}_{||}^2 s_n(\omega_0 - \bar{\omega}_n^c)/\bar{\omega}_n^c \bar{\beta}_\perp^4$ are the normalized amplitude and the frequency of the external monochromatic signal, respectively. In order to write the boundary condition (5b) at the gyrotron output (see [27] for details), we assume that the transverse structure and direction of rotation of the external signal are the same as that of the operating mode with $n = N$. For high-power gyrotrons, it can be realized based on a novel quasi-optical convertor proposed in [28]. Note that some modifications of (5b) (compared with the form obtained in [27]) are caused by the fact that the gyrofrequency changes during the gyrotron startup.

III. Simulations of 230-GHz MW-Level SH Gyrotron

Based on the developed model, we performed simulations of a high-power SH gyrotron with an operating frequency of 230 GHz. With the MW power level in mind, the fairly high transverse mode $TE_{34,14}$ was chosen as the operating one to provide an acceptable Ohmic load. In the simulation, it was assumed that the gyrotron cavity was made of copper, taking into account the possible surface roughness (i.e., the value of the skin depth was taken twice as much as that given by the known formula $d_n = (2\pi)^{-1}(c\lambda_n/\sigma)^{1/2}$, where $\sigma = 5 \cdot 10^{17}$ is the copper conductivity).

The optimized profile of the gyrotron cavity with the radius of the regular part of 18.34 mm and the length of 12 mm is shown in Fig. 1(a). Fig. 1(b) demonstrates the extremely dense spectrum of competing modes near the operating frequency. Note that for the injection radius of 7.17 mm (which corresponds to the maximum of the coupling coefficient for the operating SH mode), there are several dangerous competitors at the fundamental resonance, including modes of the equidistant spectrum $TE_{\pm 15,8}$ and $TE_{\pm 16,8}$ with higher coupling coefficients and the nearest in the magnetic field modes $TE_{18,7}$ and $TE_{\pm 6,12}$.

Note that the length of the regular part of the gyrotron cavity was significantly shortened in comparison with the value optimal for achieving the maximum SH efficiency; thus, diffractive Q-factor of the desired mode was of 2500. It was done in order to decrease the diffraction Q-factors of competing FH modes and, accordingly, to increase their starting currents [11]. Nevertheless, for the accelerating voltage of 100 kV and the pitch-factor of 1.3, the generation zone of the operating SH mode is almost completely overlapped by zones of competing FH modes (Fig. 2); thus, selective gyrotron excitation with high power at the SH in the free-running regime is not possible. However, as shown below, efficient excitation of the SH with sufficiently high efficiency and power can be provided in the regime of frequency-locking by a weak external signal.

For further simulations, the operating current was chosen equal to 50 A, since for this value, the MW level of SH generation can be reached at the $TE_{34,14}$ mode. The simplest startup scenario with a linear voltage rise in time from 75 to 100 kV was considered (Fig. 3). Note here, that in practice, the voltage rise time in long-pulse gyrotrons is on the order of milliseconds. However, a typical cavity fill time is on the order of nanoseconds. Therefore, the choice of 300 ns for describing the startup scenario looks like a reasonable scale, which is fast enough for saving the time of simulations and, at the same time, sufficiently slow for studying the physics of nonlinear processes.

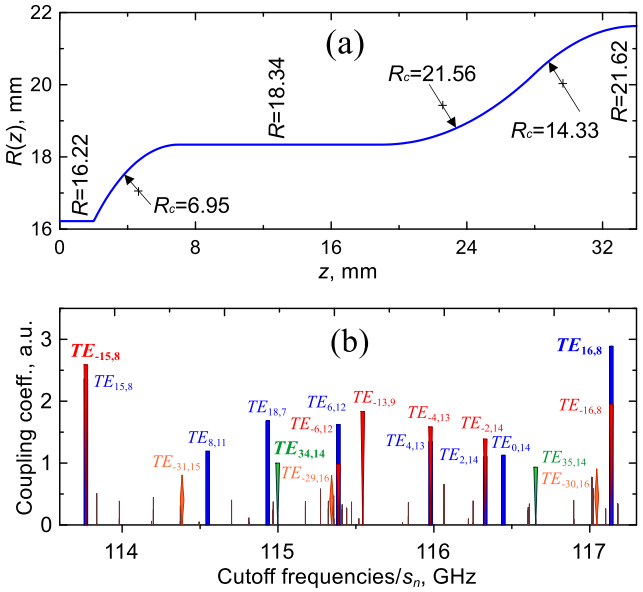

Fig. 1. (a) Optimized cavity profile of the simulated 230-GHz gyrotron. (b) Normalized coupling coefficients of the operating and competing modes (modes spectrum) for the injection radius of 7.17 mm. Blue and red lines correspond to FH modes of direct and opposite rotation. Differently rotating SH modes are marked by green and orange lines, respectively. Black lines show modes which are not important for competition.

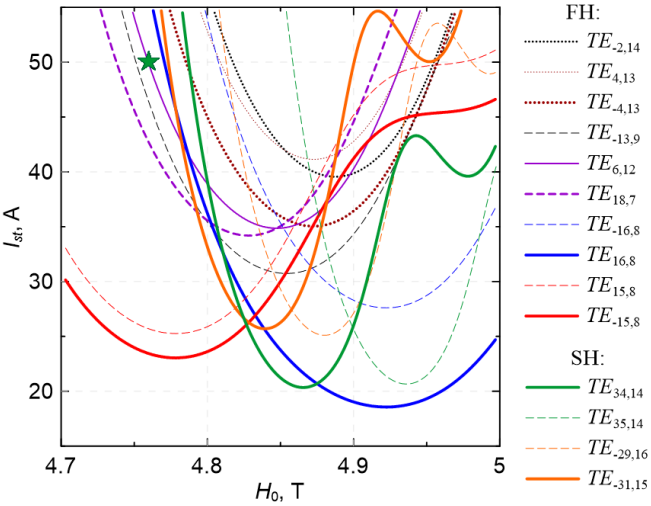

Fig. 2. Excitation zones for competing modes: the operating voltage $\bar{U} = 100$ kV and the pitch-factor $\bar{g} = 1.3$. The operating point with the maximum efficiency is marked by the green star (the guiding magnetic field of 4.76 T).

In the free-running regime, the $TE_{16,8}$ FH mode (blue line in Fig. 3) is the first which is excited on the rising front of the accelerating voltage, suppresses all other competitors, and continues to exist in a steady-state generation regime (Fig. 4) with an output power of about 1.1 MW. As a result, transverse efficiency $\eta_\perp = 1 - (2\pi)^{-1}\langle|p|^2\rangle_{\theta_0}$ is 35%; total efficiency is 22%, taking into account the Ohmic losses. Untypical low FH efficiency is explained by using the shortened cavity.

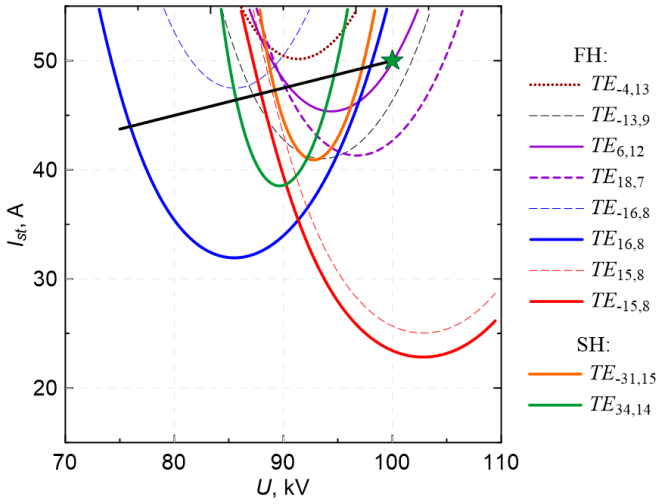

Fig. 3. Modes' excitation zones depending on the accelerating voltage for the guiding magnetic field of 4.76 T. Black line shows the current–voltage characteristics in the startup process. The operating point with maximum efficiency is marked by the green star.

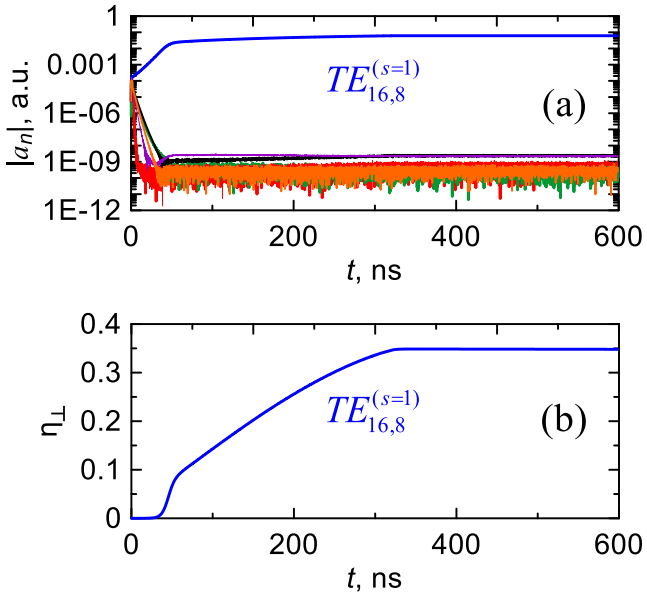

Fig. 4. Results of simulations for the free-running (autonomous) regime. (a) Temporal dependences of amplitudes of competing modes and (b) transverse efficiency are shown. The startup process ends at 300 ns.

The situation is principally different in the frequency-locking regime. In simulations, we use the external signal with a power of 50 kW (about 5% of the desired output level of 1 MW), which for the given frequency can be generated by an FH gyrotron [7]. Such signal provides priming the desirable SH mode $TE_{34,14}$ (Fig. 5), which, as a result, wins in the competition. The zone of efficient priming corresponds to hard self-excitation at the SH (Fig. 2). Note that in the operating point, the gyrotron should remain locked by the external signal and the switching off leads to the excitation of the parasitic FH $TE_{-15,8}$ mode.

According to simulations, the output power of SH generation reaches 0.95 MW (total efficiency is ~20%); the Ohmic loads on the cavity walls are of ~2.5 kBT/cm^2, which is still acceptable for water cooling.

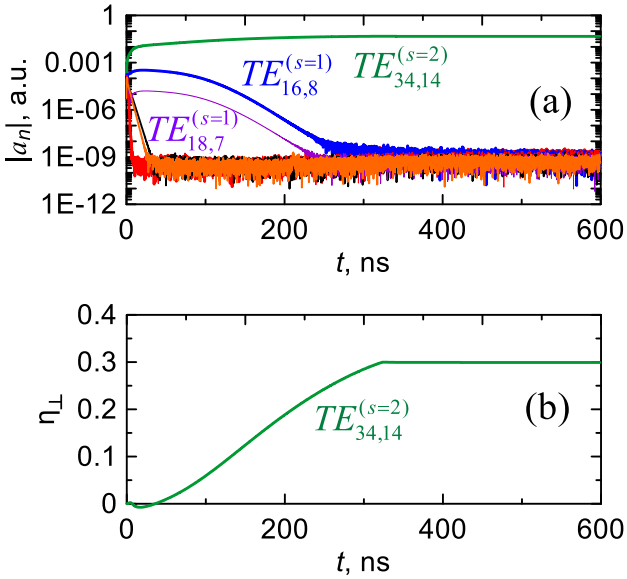

Fig. 5. Same as in Fig. 4 for simulations of the frequency-locking regime. (a) Temporal dependences of amplitudes of competing modes. (b) Transverse efficiency are shown. The startup process ends at 300 ns.

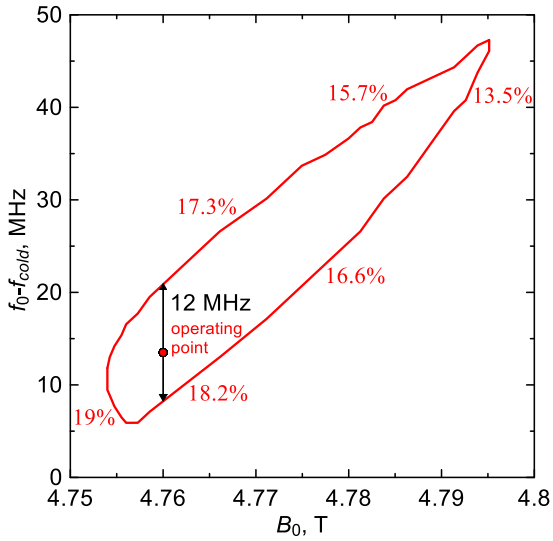

Fig. 6. Frequency-locking band versus guiding magnetic field. The output efficiency at the boundaries of the band is marked.

In Fig. 6, the dependence of frequency-locking bandwidth on the guiding magnetic field is shown. For the operating point, the frequency-locking bandwidth is about 10 MHz. This value can be doubled when the current is reduced to 45 A. However, in this case, the generation efficiency decreases to 16%, and the power, respectively, is 0.7 MW.

Note that the calculated bandwidth value is limited by competition with FH modes and, as a result, it is two times smaller than that 20 MHz given by the well-known Adler formula [29]. Moreover, this zone is at least twice as narrow as compared with the simulations at a given voltage, i.e., not taking into account the gyrotron startup.

IV. Conclusion

Thus, with a specific example, we have shown that the locking a gyrotron with an external monochromatic signal makes it possible to provide selective excitation of SH generation

at the very high-order transverse mode (much higher than in the currently known record experiments [10]). In such a way, it is possible to significantly increase in SH gyrotrons output power. However, the efficiency of SH generation remains strongly limited by competition with FH modes. Nevertheless, the proposed method may ultimately allow gyrotrons to move at a high-power level to a range of higher frequencies based on existing superconducting magnets.

REFERENCES

[1] M. Thumm, "State-of-the-art of high-power gyro-devices and free electron masers," *J. Infr., Millim., THz Waves*, vol. 41, no. 1, pp. 1–140, Jan. 2020, doi: 10.1007/s10762-019-00631-y.

[2] A. G. Litvak, G. G. Denisov, and M. Y. Glyavin, "Russian gyrotrons: Achievements and trends," *IEEE J. Microw.*, vol. 1, no. 1, pp. 260–268, Jan. 2021, doi: 10.1109/JMW.2020.3030917.

[3] R. C. Wolf *et al.*, "Electron-cyclotron-resonance heating in wendelstein 7-X: A versatile heating and current-drive method and a tool for in-depth physics studies," *Plasma Phys. Controlled Fusion*, vol. 61, no. 1, Jan. 2019, Art. no. 014037, doi: 10.1088/1361-6587/aaeab2.

[4] C. Darbos *et al.*, "Status of the ITER electron cyclotron heating and current drive system," *J. Infr., Millim., THz Waves*, vol. 37, no. 1, pp. 4–20, Oct. 2016, doi: 10.1007/s10762-015-0211-3.

[5] K. A. Avramidis *et al.*, "Overview of recent gyrotron R&D towards DEMO within EUROfusion work package heating and current drive," *Nucl. Fusion*, vol. 59, no. 6, Jun. 2019, Art. no. 066014, doi: 10.1088/1741-4326/ab12f9.

[6] S. Konovalov, "Tokamak with reactor technologies concept," in *Proc. 28th IAEA Fusion Energy Conf.*, May 2021, Art. no. P8.1157. [Online]. Available: https://conferences.iaea.org/event/214/contributions/17661/#:~:text=Description,the%20hybrid%20fusion%2Dfission%20system

[7] G. G. Denisov *et al.*, "First experimental tests of powerful 250 GHz gyrotron for future fusion research and collective Thomson scattering diagnostics," *Rev. Sci. Instrum.*, vol. 89, no. 8, Aug. 2018, Art. no. 084702, doi: 10.1063/1.5040242.

[8] T. Kariya *et al.*, "Development of high power gyrotrons for advanced fusion devices," *Nucl. Fusion*, vol. 59, no. 6, Jun. 2019, Art. no. 066009, doi: 10.1088/1741-4326/ab0e2c.

[9] A. V. Gaponov *et al.*, "Powerful millimetre-wave gyrotrons," *Int. J. Electron.*, vol. 51, no. 4, pp. 277–302, Oct. 1981, doi: 10.1080/00207218108901338.

[10] T. Saito *et al.*, "Generation of high power sub-terahertz radiation from a gyrotron with second harmonic oscillation," *Phys. Plasmas*, vol. 19, no. 6, Jun. 2012, Art. no. 063106, doi: 10.1063/1.4729316.

[11] V. E. Zapevalov, S. A. Malygin, and S. E. Tsimring, "High-power gyrotron at second harmonic of cyclotron frequency," *Radiophysics Quantum Electron.*, vol. 36, no. 6, pp. 346–353, Jun. 1993, doi: 10.1007/BF01038234.

[12] V. E. Zapevalov, V. N. Manuilov, O. V. Malygin, and S. E. Tsimring, "High-power twin-beam gyrotrons operating at the second gyrofrequency harmonic," *Radiophysics Quantum Electron.*, vol. 37, no. 3, pp. 237–240, Mar. 1994, doi: 10.1007/BF01054034.

[13] I. V. Bandurkin, A. P. Fokin, M. Y. Glyavin, A. G. Luchinin, I. V. Osharin, and A. V. Savilov, "Demonstration of a selective oversized cavity in a terahertz second-harmonic gyrotron," *IEEE Electron Device Lett.*, vol. 41, no. 9, pp. 1412–1415, Sep. 2020, doi: 10.1109/LED.2020.3010445.

[14] N. A. Zavolsky, E. V. Ilyakov, Y. K. Kalynov, I. S. Kulagin, V. N. Manuilov, and A. S. Shevchenko, "High-power relativistic milimeter-wave gyrotron operating at the second cyclotron harmonic," *Radiophysics Quantum Electron.*, vol. 61, no. 1, pp. 40–47, Jun. 2018, doi: 10.1007/s11141-018-9868-5.

[15] I. V. Bandurkin, V. L. Bratman, Y. K. Kalynov, V. N. Manuilov, I. V. Osharin, and A. V. Savilov, "High-harmonic gyrotrons with axis-encircling electron beams at IAP RAS," *Radiophysics Quantum Electron.*, vol. 62, nos. 7–8, pp. 513–519, Dec. 2019, doi: 10.1007/s11141-020-09997-9.

[16] V. S. Ergakov and M. A. Moiseev, "Theory of synchronization of oscillations in a cyclotron-resonance maser monotron by an external signal," *Radiophysics Quantum Electron.*, vol. 18, no. 1, pp. 89–97, Jan. 1975, doi: 10.1007/BF01037666.

[17] W. M. Manheimer, "Theory of the multi-cavity phase locked gyrotron oscillator," *Int. J. Electron.*, vol. 63, no. 1, pp. 29–47, Jul. 1987, doi: 10.1080/00207218708939106.

[18] G. S. Nusinovich, *Introduction to Physics of Gyrotons*. Baltimore, MD, USA: Johns Hopkins Univ. Press, 2004.

[19] V. L. Bakunin, G. G. Denisov, and Y. V. Novozhilova, "Frequency and phase stabilization of a multimode gyrotron with megawatt power by an external signal," *Tech. Phys. Lett.*, vol. 40, no. 5, pp. 382–385, May 2014, doi: 10.1134/S1063785014050034.

[20] V. L. Bakunin, G. G. Denisov, and Y. V. Novozhilova, "Principal enhancement of THz-range gyrotron parameters using injection locking," *IEEE Electron Device Lett.*, vol. 41, no. 5, pp. 777–780, May 2020, doi: 10.1109/LED.2020.2980218.

[21] I. G. Zarnitsyna and G. S. Nusinovich, "Radiophys," *Quantum Electron.*, vol. 20, pp. 313–317, Mar. 1977, doi: 10.1007/bf01039476.

[22] T. Saito *et al.*, "Observation of dynamic interactions between fundamental and second-harmonic modes in a high-power sub-terahertz gyrotron operating in regimes of soft and hard self-excitation," *Phys. Rev. Lett.*, vol. 109, no. 15, Oct. 2012, Art. no. 155001, doi: 10.1103/PhysRevLett.109.155001.

[23] A. P. Gashturi, G. S. Nusinovich, I. V. Zotova, E. S. Semenov, S. P. Sabchevski, and M. Y. Glyavin, "Nonlinear excitation of parasitic modes in harmonic gyrotrons," *Phys. Plasmas*, vol. 27, no. 6, Jun. 2020, Art. no. 063304, doi: 10.1063/5.0010593.

[24] M. Glyavin *et al.*, "Investigation of the frequency double-multiplication effect in a sub-THz gyrotron," *J. Infr., Millim. THz Waves*, vol. 41, no. 10, pp. 1245–1251, 2020, doi: 10.1007/s10762-020-00726-x.

[25] V. N. Manuilov and M. Y. Glyavin, "Synthesis of current–voltage characteristics of 670 GHz gyrotron magnetron injection gun and calculation of the helical electron beam parameters at the leading edge of a high-voltage pulse," *J. Infr., Millim., THz Waves*, vol. 34, no. 2, pp. 119–126, Feb. 2013, doi: 10.1007/s10762-012-9953-3.

[26] M. Y. Glyavin, A. L. Goldenberg, A. N. Kuftin, V. K. Lygin, A. S. Postnikova, and V. E. Zapevalov, "Experimental studies of gyrotron electron beam systems," *IEEE Trans. Plasma Sci.*, vol. 27, no. 2, pp. 474–483, Apr. 1999, doi: 10.1109/27.772276.

[27] N. S. Ginzburg, A. S. Sergeev, and I. V. Zotova, "Time-domain self-consistent theory of frequency-locking regimes in gyrotrons with low-Q resonators," *Phys. Plasmas*, vol. 22, no. 3, Mar. 2015, Art. no. 033101, doi: 10.1063/1.4913672.

[28] A. V. Chirkov, G. G. Denisov, and A. N. Kuftin, "Perspective gyrotron with mode converter for co- and counter-rotation operating modes," *Appl. Phys. Lett.*, vol. 106, no. 26, Jun. 2015, Art. no. 263501, doi: 10.1063/1.4923269.

[29] R. Adler, "A study of locking phenomena in oscillators," *Proc. IRE*, vol. 34, no. 6, pp. 351–357, Jun. 1946, doi: 10.1109/JRPROC.1946.229930.